Well posed reconstruction of the solar coronal magnetic field

T. Amari[1], T. Z. Boulmezaoud[2], and J. J. Aly[3]

[1] CNRS, Centre de Physique Théorique de l'Ecole Polytechnique, 91128 Palaiseau Cedex, France
   e-mail: amari@cpht.polytechnique.fr
[2] Laboratoire de Mathématiques, Université de Versailles Saint-Quentin-en-Yvelines
   Bâtiment Fermat, 45 avenue des Etats-Unis - 78035 Versailles, France
[3] AIM - Unité Mixte de Recherche CEA - CNRS - Université Paris VII - UMR No 7158, Centre d'Études de Saclay,
   91191 Gif sur Yvette Cedex, France

ABSTRACT

We present and compare two methods for the reconstruction of the solar coronal magnetic field, assumed to be force-free, from photospheric boundary data. Both methods rely on a well posed mathematical boundary value problem and are of the Grad-Rubin type, i.e., the couple $(\boldsymbol{B}, \alpha)$ is computed iteratively. They do differ from each other on the one hand by the way they address the zero-divergence of $\boldsymbol{B}$ issue, and on the other hand by the scheme they use for computing α at each iteration. The comparison of the two methods is done by numerically computing two examples of nonlinear force-free fields associated to large scale strong electric current distributions, whose exact forms can be otherwise determined semi-analytically. In particular, the second solution has a large nonlinearity even in the weak field region – a feature which is not present in the actual magnetograms, but is interesting to consider as it does allow to push the methods to the limits of their range of validity. The best results obtained with those methods give a relative vector error smaller than 0.01. For the latter extreme case, our results show that higher resolution reconstructions with bounded convergence improve the approximated solution, which may be of some interest for the treatment of the data of future magnetographs.

Key words. Sun: magnetic fields – Sun: corona

1. Introduction

It is well known that a large part of the low solar corona is dominated by the magnetic field $\boldsymbol{B}$ which is created inside the sun by a dynamo process and then emerges into the atmosphere. This magnetic field plays an important role in most structures and phenomena observed at various wavelengths such as prominences, small and large scale eruptive events, and continuous heating of the plasma, and therefore it is important to understand its three-dimensional properties in order to elaborate efficient theoretical models. Unfortunately, the magnetic field is difficult to measure locally in the hot and tenuous corona. But this can be done at the level of the cooler and denser photosphere, and several instruments with high resolution vector magnetographs are currently available (THEMIS, Imaging Vector Magnetograph (IVM), the Advanced Stokes Polarimeter (ASP)), or will be shortly available (SOLIS, and future programmed missions such as SOLAR-B, SOLAR-ORBITER, Solar Dynamics Observatory (SDO)). This has lead solar physicists to develop an approach which consists in *reconstructing* the coronal magnetic field from boundary data given on the photosphere.

The problem then consists in solving the set of equilibrium equations of magnetohydrodynamics (MHD) for given boundary conditions. Actually, some more specific assumptions are usually added for making the problem tractable, and what is really considered is a model in which the field is taken, e.g., to be potential, linearly or nonlinearly force-free, or to obey linear magnetohydrostatics. In particular, the nonlinear force-free case has been the subject of much work, which has lead to the appearance of many conceptually different methods of reconstruction: Grad-Rubin like methods (Sakurai 1981; Amari et al. 1997, 1999; Wheatland 2004), based on a scheme originally proposed by Grad & Rubin (1958), MHD methods (Mikic & McClymont 1994), Stress-Relax method (Roumeliotis 1996; Valori et al. 2005), Relaxation methods (Chodura & Schluter 1981; Wiegelmann & Neukirch 2003), Optimisation methods (Wheatland et al. 2000; Wiegelmann & Neukirch 2003), Boundary Element method (Yan & Sakurai 2000), and Vertical Integration method (VIM) (Wu et al. 1990; Cuperman et al. 1991; Demoulin et al. 1992). It is important to note that, although the three components of the magnetic field are measured on the sun surface, only part of this information – e.g., the normal components of the force-free field $\boldsymbol{B}$ and of the electric current – can be imposed on the boundary in order to get a well set boundary value problem (BVP) for the mixed elliptic-hyperbolic system obeyed by $\boldsymbol{B}$ and the force-free function α (Aly 1989; Amari et al. 1998, 1997; Low 2005). Although regularization procedures have been successfully developed in the linear force-free case (Amari et al. 1998) for the ill-posed

formulation associated to VIM (Wu et al. 1990; Cuperman et al. 1991; Demoulin et al. 1992), the corresponding non-linear case still remains non-regularised. It should also be noticed that is is important for each method to distinguish between the continuous BVP it does start with and the discrete BVP which is actually solved on a computer.

In this paper, we are interested in the reconstruction problem for a nonlinear force-free field by two methods of the Grad-Rubin type that we call XTRAPOL and FEMQ, respectively. For them, rigorous existence and partial uniqueness have been proved (Bineau 1972; Boulmezaoud & Amari 2000), and they are then based on a well posed BVP. We would like in particular to address several remaining issues concerning the discrete problem. The first important one is the treatment of the well known div $\boldsymbol{B} = 0$ constraint, which still represents a serious challenge in the development of numerical MHD schemes. A possible approach is to work with a vector potential $\boldsymbol{A}$ associated to the magnetic field $\boldsymbol{B}$ with a staggered mesh such that the approximate solution lies in the functional space that is in the kernel of the div operator. This is the approach followed in Amari et al. (1999), where we first introduced the code XTRAPOL based on a finite difference scheme. A different approach avoiding the introduction of $\boldsymbol{A}$ consists in working in a functional space corresponding to div $\neq 0$ Q1 finite elements, and to minimize div B in the least square sense for the associated $\boldsymbol{curl} -$ div system corresponding to the elliptic Biot-Savart problem. It is adopted in the second method, FEMQ, presented here. The second issue concerns the computation of the force-free function α (which is constant along the field lines) at each iteration. This is done by following the characteristics (field lines) in XTRAPOL, or by solving an hyperbolic linear system in FEMQ.

To compare these two methods we consider the well known particular class of force-free fieds derived in Low & Lou (1991) (referred to hereafter as LowLou solution) and generate two particular solutions corresponding to two sets of parameters. Those solutions are associated to a large scale strong enough electric current distribution. The second solution is introduced to push the methods to the limits of their range of validity since the nonlinearities are on a large scale including weak field region. It is worth noticing that the boundary conditions provided by the LowLou solution differs from actual data in the sense that they generally lead to a distribution of α with a support of the order of or larger than that of B_n, while in general vector magnetograms show electric currents more concentrated than B_n. This remark implies that since in Amari et al. (1999) $B_n = 0$ and $\alpha = 0$ on the numerical boundaries other than $\{z = 0\}$, one has to choose a large box and to reduce as well the error estimates to a smaller inner box. While $\alpha \neq 0$ on 5 boundaries for the LowLou solutions, no connection from those boundaries to strong field region could be found for the approximated solution, because α is constant along field lines. In the present paper we introduce a method to deal with non zero B_n and α on all boundaries for XTRAPOL, which implies some technical approach to achieve continuity of the vector potential on the edge of the computational box.

Finally we would like to inform the reader that an interesting comparison study of several other reconstruction methods on the same exact solutions, using the same error diagnostics have been independently performed in Schrijver et al. (2005). It is worth noting however that the computations performed in Schrijver et al. (2005) with an implementation of XTRAPOL that does not address the above issues of $B_n \neq 0$ and $\alpha \neq 0$ on the five outer boundaries,(as well as other issues presented in the next sections), may not be suited for test cases such as those considered in the present paper. This is however not the case for solar magnetogram like data of an isolated active region placed in a large box with no magnetic flux outside, and for which from multiwavelength observations, there is apparently no magnetic connection with other active regions out of the field of view, as done in Bleybel et al. (2002); Régnier et al. (2002); Régnier & Amari (2004). Furthermore it is important to note that in order to be meaningful, the two methods presented in the present paper are compared with the corresponding LowLou solution, for exactly the same boundary conditions applied on the five outer boundaries even for the second test case (unlike in Schrijver et al. (2005) where various type of boundary conditions have been considered for this case). It is indeed well known that the mixed elliptic-hyperbollic nature of the force-free equations requires boundary conditions that strongly affect the nature of the solution inside the domain, especially in the case of a relatively small box. Therefore, comparing the figures obtained in this paper with those obtained in Schrijver et al. (2005) is rigorously meaningful for the first test case only.

The paper is organized as follows. We first introduce in Sect. 2.1 the BVP that is to be solved and the general Grad-Rubin scheme which is the ground of our methods. In Sects. 3 and 4, respectively, we present XTRAPOL and FEMQ. The two particular solutions used to compare those methods are then presented in Sect. 5, while comparison results as well as dependency on the numerical resolution are presented in Sect. 6. Section 7 gather some concluding remarks.

2. Mathematical framework

2.1. The boundary value problem

In the model we consider in this paper, the corona and the photosphere are represented by the half-space $\Omega = \{z > 0\}$ and the plane $\partial\Omega = \{z = 0\}$, respectively. Ω is assumed to be filled up with a low beta slightly resistive and viscous plasma embedded in a magnetic field $\boldsymbol{B}$ which is taken to be force-free and to decrease sufficiently fast to zero at infinity. Therefore, it does obey the equations

$$\boldsymbol{\nabla} \times \boldsymbol{B} = \alpha\boldsymbol{B}, \tag{1}$$
$$\boldsymbol{\nabla} \cdot \boldsymbol{B} = 0. \tag{2}$$

It results at once from Eqs. (1) and (2) that the function α satisfies the constraint

$$\boldsymbol{B} \cdot \boldsymbol{\nabla}\alpha = 0 \tag{3}$$

which merely states that α keeps a constant value along any field line.

The set of Eqs. (1) and (2) has a mixed elliptic-hyperbolic structure. Basically, it can be decomposed into an elliptic part

for $\boldsymbol{B}$ (at α given), and an hyperbolic one for α (at $\boldsymbol{B}$ given), associated with Eq. (3). To solve for the elliptic part, one should give the normal component B_n of the magnetic field on $\partial\Omega$, while to solve for the hyperbolic one, Eq. (3) indicates that the value of α should be given on the part $\partial\Omega^+$ of $\partial\Omega$ where $B_n > 0$, say. This leads us to consider the BVP first introduced by Grad & Rubin (1958). It consists of Eqs. (1)−(3) along with the boundary conditions

$$B_n|_{\partial\Omega} = b_0, \tag{4}$$
$$\alpha|_{\partial\Omega^+} = \alpha_0, \tag{5}$$

where b_0 and α_0 are two given regular functions, and the asymptotic condition

$$\lim_{|r|\to\infty} |\boldsymbol{B}| = 0. \tag{6}$$

In the numerical practice, we need to consider instead of the upper half-space the bounded domain $\Omega_b = [x0, x1] \times [y0, y1] \times [z0, z1]$. Then the asymptotic condition (6) is no longer useful and the boundary conditions (4)−(5) are imposed on the whole $\partial\Omega_b$.

2.2. Principle of the Grad-Rubin method

In the Grad-Rubin method, the BVP above is solved iteratively, with its elliptic and hyperbolic parts being solved successively at each step. More precisely, we look for a sequence $(\boldsymbol{B}^{(n)}, \alpha^{(n)})$ solution of – BVP-GR hereafter –

$$\boldsymbol{B}^{(n)}.\boldsymbol{\nabla}\alpha^{(n)} = 0 \quad \text{in} \quad \Omega_b, \tag{7}$$
$$\alpha^{(n)}|_{\partial\Omega_b^+} = \alpha_0, \tag{8}$$

and

$$\boldsymbol{\nabla} \times \boldsymbol{B}^{(n+1)} = \alpha^{(n)}\boldsymbol{B}^{(n)} \quad \text{in} \quad \Omega_b, \tag{9}$$
$$\boldsymbol{\nabla} \cdot \boldsymbol{B}^{(n+1)} = 0 \quad \text{in} \quad \Omega_b, \tag{10}$$
$$B_z^{(n+1)}|_{\partial\Omega_b} = b_0. \tag{11}$$

The iteration process is initialized by choosing for $\boldsymbol{B}^{(0)}$ the unique solution of

$$\boldsymbol{\nabla} \times \boldsymbol{B}^{(0)} = 0 \quad \text{in} \quad \Omega_b, \tag{12}$$
$$B_z^{(0)}|_{\partial\Omega_b} = b_0. \tag{13}$$

2.3. Some mathematical results

We next recall some general results on the BVP set either in Ω or in Ω_b:

- For the unbounded domain $\Omega = \{z > 0\}$ no existence theorem has yet been proven. However, it seems quite likely that there is always a solution, at least when α is choosen not too large, a guess which is reinforced by the proof of existence recently given in Kaiser et al. (2000) for the case where the problem is set in an exterior domain – e.g., the exterior of a sphere – rather than in a half-space.
- For the bounded domain Ω_b and α_0 not too large, an existence theorem has been proved (Bineau 1972) for the solutions in a Hölder functional space (set of functions

sufficiently regular and whose derivatives are also regular enough, (Brezis 1983)) under the additional assumption that $\boldsymbol{B}$ has a simple magnetic topology (this means in particular that $\boldsymbol{B}$ should not vanish in Ω). This theorem has been extended to more general spaces $((\alpha, \boldsymbol{B}) \in L^\infty \times H^1(\Omega_b))$, which allows for solutions admitting null points and separatrix surfaces (Boulmezaoud & Amari 2000).

- When α_0 is not too large, uniqueness and continuity of the solutions with respect to the boundary conditions have been shown to occur in the bounded domain Ω_b (Bineau 1972) under the topological condition quoted above.

It is worth noticing that these results are established by proving the convergence of the Grad-Rubin procedure – an important point for grounding safely the two numerical methods that we present now.

3. Finite differences-characteristics approach: XTRAPOL

This approach has been presented in Amari et al. (1999). Therefore we just recall the basics of the approximation, giving details only for the improvements we have introduced.

3.1. Introduction of the potential vector

To address the div $B = 0$ constraint, XTRAPOL uses a vector-potential formulation with a particular gauge defined by

$$\boldsymbol{B} = \boldsymbol{\nabla} \times \boldsymbol{A} \quad \text{in} \quad \Omega_b, \tag{14}$$
$$\boldsymbol{\nabla} \cdot \boldsymbol{A} = 0 \quad \text{in} \quad \Omega_b, \tag{15}$$
$$\boldsymbol{\nabla}_t \cdot \boldsymbol{A}_t = 0 \quad \text{on} \quad \partial\Omega_b, \tag{16}$$

where the subscript t in ξ_t stands for the trace (when it exists) of the tangential component on the boundary of the operator or the field ξ. As noted in Amari et al. (1999), this gauge implies that

$$\partial_n A_n = 0 \quad \text{on} \quad \partial\Omega_b, \tag{17}$$

where $\partial_n f = \hat{n} \cdot \boldsymbol{\nabla} f$.

3.2. BVP for $\boldsymbol{A}$: BVP-A

In the vector potential formulation, the iteration on $\boldsymbol{B}$ translates into an iteration on $\boldsymbol{A}$. $\boldsymbol{A}^{(n+1)}$ is a vector field belonging to the space $[C^2(\Omega_b) \cup C^1(\partial\Omega_b)]^3$ which solves BVP-A defined by

$$-\Delta\boldsymbol{A}^{(n+1)} = \alpha^{(n)}\boldsymbol{\nabla} \times \boldsymbol{A}^{(n)} \quad \text{in} \quad \Omega_b, \tag{18}$$
$$\boldsymbol{A}_t^{(n+1)} = \boldsymbol{\nabla}_t^\perp\chi \quad \text{on} \quad \partial\Omega_b, \tag{19}$$
$$\partial_n A_n^{(n+1)} = 0 \quad \text{on} \quad \partial\Omega_b, \tag{20}$$

where χ is a function whose existence – up to an additive constant – is an immediate consequence of Eq. (16). This BVP is discretized using finite differences on a non uniform staggered Cartesian mesh. This implies that the discretized operator $\boldsymbol{curl}_h$ is in the kernel of div_h, whence $\text{div}_h \boldsymbol{B} = 0$ up to round off errors.

As remarqued in Amari et al. (1999), the vector potential is uniquely determined in the chosen gauge at each step. However, the proof that

$$\forall n \geq 1, \boldsymbol{A}^{(n)} \quad \text{satisfies} \quad \boldsymbol{\nabla} \cdot \boldsymbol{A}^{(n)} = 0 \quad \text{in} \quad \Omega_b$$

rests on the condition that $\nabla \cdot (\alpha^{(n)} \nabla \times A^{(n)}) = 0$. Although commutativity of the various operators is analytically fullfilled (which leads to $\nabla \times A^{(n)} . \nabla \alpha^{(n)} = 0$ in Ω_b), in general vanishing of $\nabla \cdot (\alpha^{(n)} \nabla \times A^{(n)})$ is not exactly obtained numerically due to the interpolation of the products of terms which are not collocated. Therefore, we introduce a first "divergence cleaning" step by setting

$$\hat{J}^{(n)} = J^{(n)} + \nabla P^{(n)}, \tag{21}$$

where

$$J^{(n)} = \alpha^{(n)} \nabla \times A^{(n)}. \tag{22}$$

Imposing $\nabla \cdot \hat{J}^n = 0$ then leads to the BVP for $P^{(n)}$

$$-\Delta P^{(n)} = \nabla \cdot J^{(n)} \qquad \text{in} \qquad \Omega_b, \tag{23}$$

$$\partial_n P^n = 0 \qquad \text{on} \qquad \partial\Omega_b. \tag{24}$$

This step allows to get $\nabla \cdot A = 0$ to a high level of accuracy, 10^{-9} compared to 10^{-2} in Amari et al. (1999).

3.3. Normal component of B

Next we consider the problem of the determination of the function χ appearing in Eq. (19). Clearly, it has to be a solution to

$$-\Delta_t \chi = b_0 \qquad \text{on} \qquad \partial\Omega_b, \tag{25}$$

but we need also a boundary condition to get it. To discuss this point, we write $\partial\Omega_b = \bigcup_{(1 \le i \le 6)} \Gamma_i$, with Γ_i denoting its six plane faces, convening that $\Gamma_1 = \{z = z_0\}$.

In Amari et al. (1999), we imposed $\partial_n \chi = 0$ on $\partial\Gamma_1$, which was possible because we had $B_n = 0$ for $2 \le i \le 6$ (the general constraint $\int_{\Omega_b} B_n \, ds = 0$ resulting from div $B = 0$ reduces indeed in that case to $\int_{\Gamma_1} B_n \, ds = 0$, which is just the compatibility condition for the homogeneous Neumann problem for χ on Γ_1). With the assumptions made in this Paper, $B_n \ne 0$ on each face Γ_i in general, and a Neumann condition on χ cannot be set on each $\partial\Gamma_i$, for $1 \le i \le 6$, since $\int_{\Gamma_i} B_n \, ds \ne 0$, for $1 \le i \le 6$. The whole boundary $\partial\Omega_b$ must be treated as a unique domain on which χ is a solution to a BVP which consists of Eq. (25) and a boundary condition implying that $A_t = \nabla_t^\perp \chi$ is the trace of a vector potential satisfying some continuity conditions on the twelve edges $e_{i,j} = \Gamma_i \bigcap \Gamma_j$, for $1 \le (i, j) \le 6$. This implies imposing in the Lipschitzian domains (Buffa & Ciarlet 2001) continuity on χ and some compatibility conditions on the derivatives on each edge expressing the continuity of A. We achieve those conditions numerically on our mesh up to $10^{-11} - 10^{-13}$ for the numerical resolutions considered in this Paper.

3.4. BVP for α: BVP-α

Unlike in Amari et al. (1999) where we introduced a two-level iteration procedure for imposing α on the boundary of the domain, we keep here only the inner Grad-Rubin iteration loop. Using our vector potential formulation, Eqs. (7) and (8) may be rewritten as

$$\nabla \times A^{(n)} . \nabla \alpha^{(n)} = 0 \qquad \text{in} \qquad \Omega_b, \tag{26}$$

$$\alpha^{(n)}|_{\partial\Omega_b^+} = \alpha_0. \tag{27}$$

As remarqued above, unlike in Amari et al. (1999), no iteration loop is introduced for imposing a fraction of α.

The characteristics $(X; s)$ is a solution of (Amari et al. 1999)

$$X' = B(X), \tag{28}$$

$$X(0) = q, \tag{29}$$

for q given in Ω_b (the prime symbol standing for differentiation with respect to the parameter that runs along the characteristics). Then for any node $q_h \in \Omega_b$ at which α is defined, one gets α_h as

$$\alpha(q_h) = \alpha_0(X_{\partial\Omega_b^+}(q_h)), \tag{30}$$

where $X_{\partial\Omega_b^+}(q_h) = X(q_h, s_{\partial\Omega_b^+})$ is the intersection of $\{X(q; s) : s < 0\}$ with $\partial\Omega_b^+$. Since α_0 is known at nodes that do not in general coincide with $X_{\partial\Omega_b^+}(q_h)$, we use an interpolation from its four nearest neighbors.

Unlike in Amari et al. (1999), α is not defined on the cell faces but rather on the cell vertices. From our experience on reconstructing coronal magnetic fields from actual vector magnetograph data (Bleybel et al. 2002; Régnier et al. 2002; Régnier & Amari 2004), we found that using one of the two methods of Amari et al. (1999) (with interpolation inside the domain while going backwards along the characteristics) has a smoothing effect which may reduce accuracy on data varying on a small scale. We therefore use a high order Adams-Bashford integration scheme with adaptive step size, which also allows us to capture the ending point of the characteristics defining the limits of the computational box. This method turns out to be slightly slower than the two ones used in Amari et al. (1999), but much better accuracy is obtained.

We have improved our convergence criterion compared to Amari et al. (1999) where the Grad-Rubin iteration loop was fixed to 4, while the outer iteration loop (which imposes a fraction of α_0 on the boundary) was fixed to 20. We now use the following convergence criterion for the sequence of B^n:

$$\frac{\| B^{(n+1)} - B^{(n)} \|_{L^2(\Omega_b)}}{\| B^{(n)} \|_{L^2(\Omega_b)}} < \epsilon, \tag{31}$$

with $\epsilon = 10^{-6}$.

As it will be shown in Sect. 6, a total number of iterations of about $30-50$ is sufficient to achieve convergence in most of the cases. Moreover, the stopping criteria is robust independently of the data put as boundary conditions. Thus it is not necessary to introduce the outer iteration loop of Amari et al. (1999), which leads to a total number of iterations of 80.

4. Finite elements approach: FEMQ

We consider now a second approach to BVP-GR. We present successively the steps for obtaining, respectively, α and B.

4.1. BVP for α

The method of characteristics presented above has some drawbacks: It requires a certain level of smoothness of the field B,
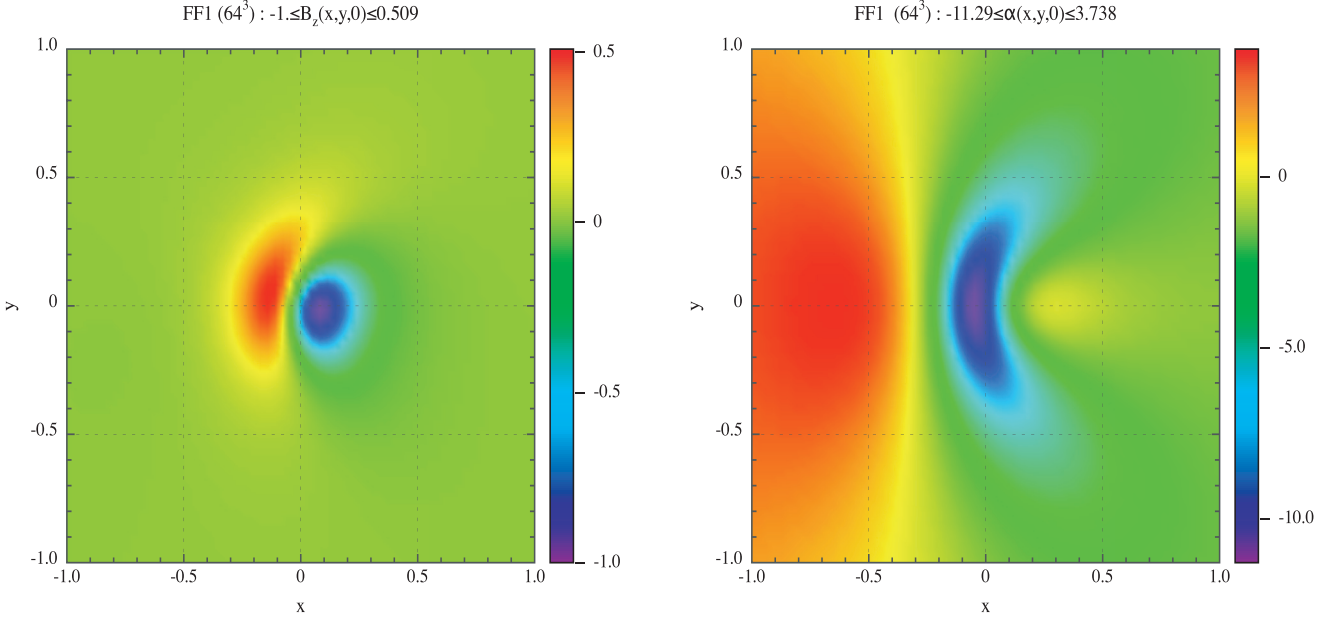
FF1 (64^3) : $-1.\leq B_z(x,y,0)\leq 0.509$

FF1 (64^3) : $-11.29\leq\alpha(x,y,0)\leq 3.738$

Fig. 1. Distributions of B_z and α on the plane $\{z = 0\}$ for the particular force-free solution FF1 (see text). α is not too small and varies on a larger scale than B_z.
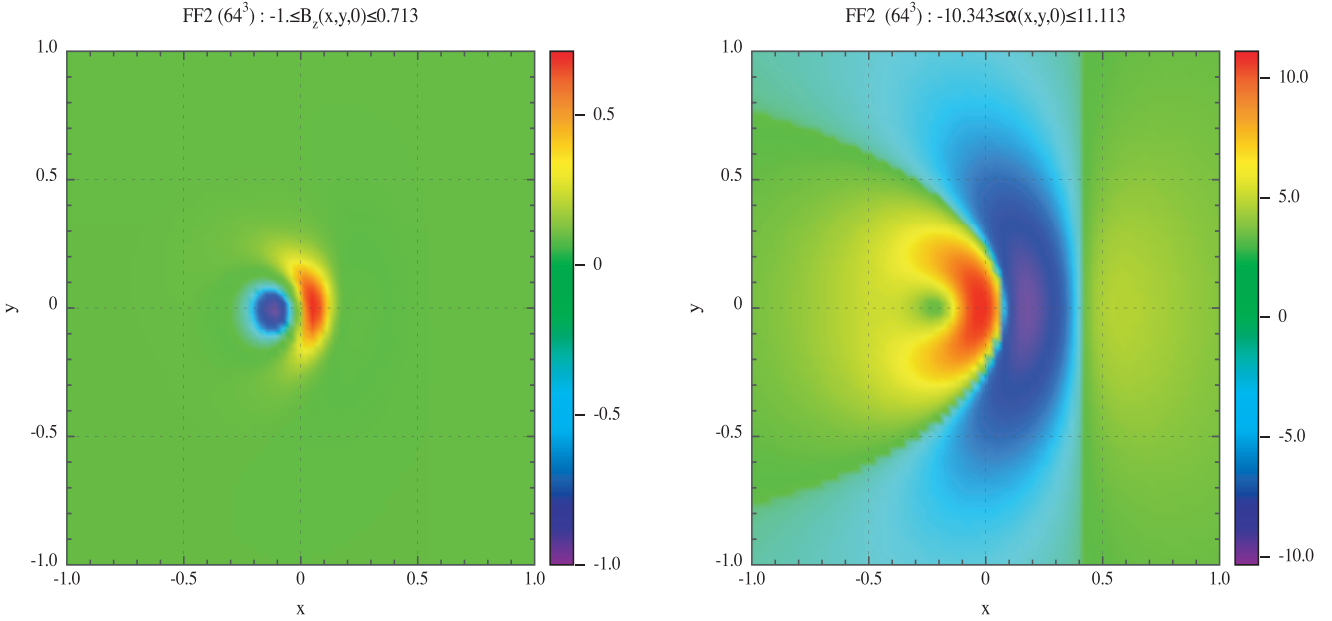
FF2 (64^3) : $-1.\leq B_z(x,y,0)\leq 0.713$

FF2 (64^3) : $-10.343\leq\alpha(x,y,0)\leq 11.113$

Fig. 2. Distributions of B_z and α on the plane $\{z = 0\}$ for the particular force-free solution FF2 (see text). This solution corresponds to an extreme test case in which B_z is much more concentrated than α. This corresponds to large electric currents on a large scale, a feature actually rarely observed on vector magnetograms.

and, while being very accurate from the computational point of view, it can be very time consuming. Certainly, it could be parallelized (this is formally possible, unlike for BVP-A), but this would require some effort since the basic integration scheme for following backwards a characteristics can be sequentially only. A (non-obvious) solution could be to perform a domain decomposition of Ω_b in P cubic domains Ω_b^P where P is also the number of processors. One then computes α in each Ω_b^P, which must however have precise knowledge of the global quantity $\boldsymbol{B}$ in Ω_b, and not only its restriction to Ω_b^P since going along a characteristics is not an operation local to Ω_b^P but a global one.

For those reasons, we consider an algorithm in which α is the solution of the linear hyperbolic system

$$\boldsymbol{B}^{(n)} \cdot \nabla\alpha^{(n)} + \epsilon^{(n)}\alpha^{(n)} = 0, \qquad \text{in} \qquad \Omega_b, \qquad (32)$$

$$\alpha^{(n)}|_{\partial\Omega_b^+} = \alpha_0, \qquad\qquad (33)$$

where $(\epsilon^{(n)})_{n\geq 0}$ is a decreasing sequence of strictly positive real numbers tending towards zero (Boulmezaoud & Amari 2001). It is worth noticing that we could also add on the RHS of Eq. (32) the term $\epsilon^{(n-1)}\alpha^{(n-1)}$, the limits of the sequences of solutions satisfying also (assuming its convergence) $\boldsymbol{B}_l \cdot \nabla\alpha_l = 0$.

The BVP above is solved by a Q1 Finite Elements discretization, using the functional space $W_h = \{u \in H^1(\Omega_b)^3 : u \mid_K \in P_k(K), \forall K \in T_k\}$, where T_k is the triangulation of the domain (here hexahedraes) – see Brezis (1983) for a definition of the functional spaces. The discretized problem then reduces to

$$a_1(\alpha_h^{(n)}, v_h) = l_1(v_h) \quad \forall v_h \in W_h, \tag{34}$$

where

$$a_1(\alpha, v) = (\boldsymbol{B}^{(n)} \cdot \nabla\alpha + \epsilon^{(n)}\alpha, v) - \int_{\partial\Omega_+} \alpha v b_0 \, \mathrm{d}\omega, \tag{35}$$

$$l_1(v) = -\int_{\partial\Omega_+} \alpha_0 v b_0 \, \mathrm{d}\omega. \tag{36}$$

In these expressions, (u, v) stands for the scalar product in $H^1(\Omega_b)^3$. We are thus lead to a non-symmetric linear system, that we solve using an iterative method (BICGSTAB).

4.2. BVP for *B*

Instead of introducing a vector potential as in the previous section, we compute here $\boldsymbol{B}^{(n+1)} = \boldsymbol{b}^{(n+1)} + B^{(0)}$ at each iteration by solving the *curl* − div system

$$\nabla \times \boldsymbol{b}^{(n+1)} = \alpha^{(n)}\boldsymbol{B}^{(n)} + \nabla p^{(n)}, \tag{37}$$

$$\nabla \cdot \boldsymbol{b}^{(n+1)} = 0, \tag{38}$$

$$\boldsymbol{b}^{(n+1)} \cdot \hat{n} = 0. \tag{39}$$

As the function P in the previous section, the unknown $p^{(n)}$ is introduced to make the RHS of Eq. (37) divergence-free, and it is a solution to the BVP

$$\Delta p^{(n)} = -\boldsymbol{\nabla} \cdot (\alpha^{(n)}\boldsymbol{B}^{(n)}) = \epsilon^{(n)}\alpha^{(n)} \text{ in } \Omega_b, \tag{40}$$

$$p^{(n)} = 0 \text{ on } \partial\Omega_b. \tag{41}$$

Existence of a solution to the original BVP for $(\boldsymbol{B}, \alpha)$ as the limit of sequences of BVP above is shown in Boulmezaoud & Amari (2000).

The first BVP (*curl* − div system) is solved by using a finite elements discretization on non divergence-free finite elements, which amounts to consider the equivalent system

- $\forall \boldsymbol{w} \in V$:

$$(\nabla \times \boldsymbol{b}^{(n+1)}, \nabla \times \boldsymbol{w}) + (\nabla \cdot \boldsymbol{b}^{(n+1)}, \nabla \cdot \boldsymbol{w}) = (\alpha^{(n)}\boldsymbol{B}^{(n)}, \nabla\boldsymbol{w}), \tag{42}$$

- $\forall \phi \in H_0^1$:

$$(\nabla p^{(n)}, \nabla\phi) = -(\alpha^{(n)}\boldsymbol{B}^{(n)}, \nabla\phi). \tag{43}$$

The first problem (which actually minimizes the div *B* term in the variational formulation) is solved using the finite elements subspace $V_h \subset V$ defined by $V_h = \{\boldsymbol{v} \in C^0(\bar{\Omega}_b)^3; \boldsymbol{v} \mid_k$ is affine, $\forall k; \boldsymbol{v}(M_j) \cdot \hat{n} = 0, \forall M_j \in \partial\Omega_b\}$, with Ω_b discretized by a triangulation consisting of hexaedres. With a basis $\{\boldsymbol{v}_h\}$ of V_h one then solves

$$a_2(\boldsymbol{b}^{(n+1)}, \boldsymbol{v}_h) = (\alpha^{(n)}\boldsymbol{B}^{(n)}, \nabla \times \boldsymbol{v}_h) \quad \forall \boldsymbol{v}_h \in V_h, \tag{44}$$

with the bilinear form a_2 defined by

$$a_2(\boldsymbol{u}, \boldsymbol{v}) = (\nabla \times \boldsymbol{u}, \nabla \times \boldsymbol{v}) + (\nabla \cdot \boldsymbol{u}, \nabla \cdot \boldsymbol{v}). \tag{45}$$
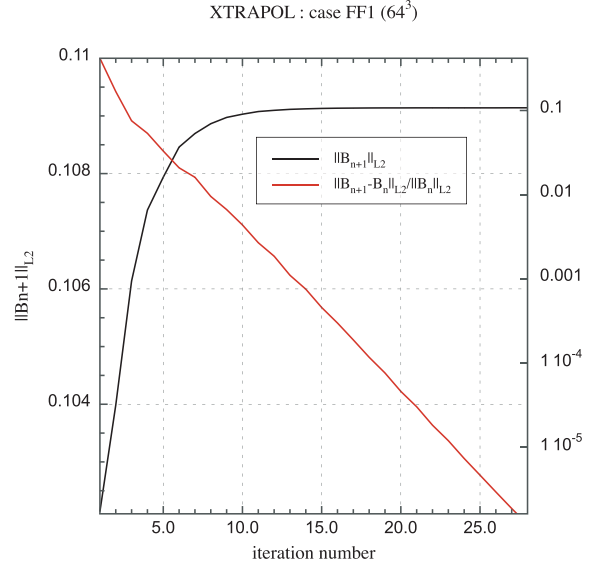

Fig. 3. Convergence properties of the method XTRAPOL applied to case FF1 with numerical resolution of 64^3. The rate of convergence of the sequences is close to exponential. The norm of the solution has reached its asymptotic value in about 15 iterations.
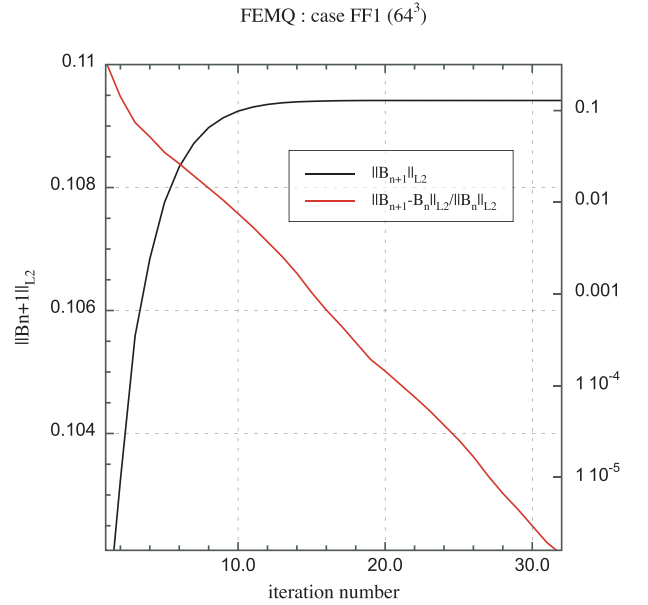

Fig. 4. Convergence properties of the method FEMQ applied to case FF1 with numerical resolution of 64^3. The rate of convergence of the sequences is close to exponential as for XTRAPOL, and the norm of the solution has reached its asymptotic value in about 15 iterations.

We thus end up with a linear algebraic system with a unique solution $\boldsymbol{b}^{(n+1)}$.

Equation (43) is a Dirichlet elliptic problem. It is solved as a Poisson equation with an iterative solver. As in the finite differences-characteristics method, the sequences of BVPs are solved until convergence is reached, with convergence being defined in the L^2 sense by Eq. (31).
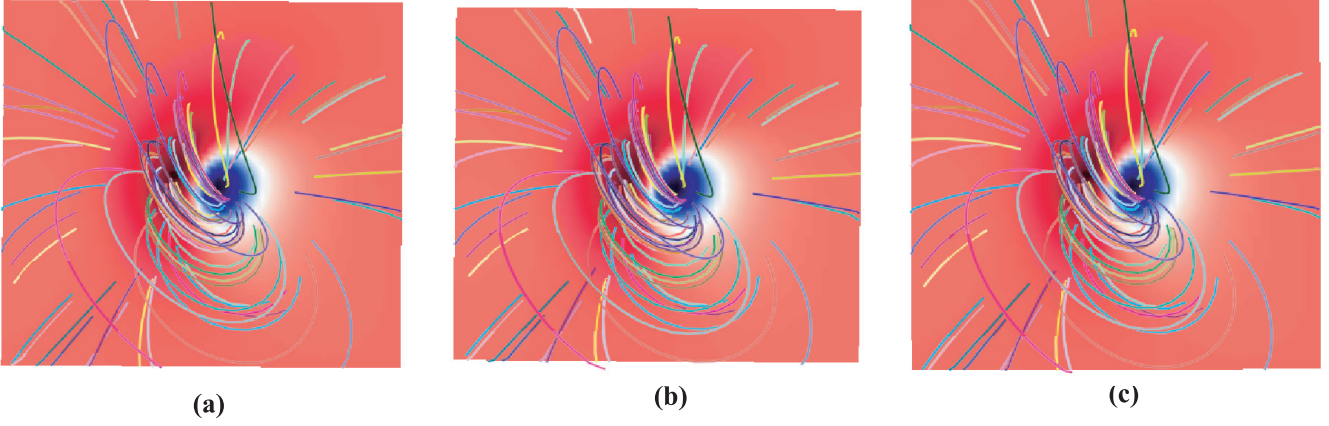
Fig. 5. Comparison of some field lines of the configurations corresponding to the case FF1 (panel **a**)) obtained with XTRAPOL (panel **b**)) and FEMQ (panel **c**)) for the same numerical resolution of 64^3.
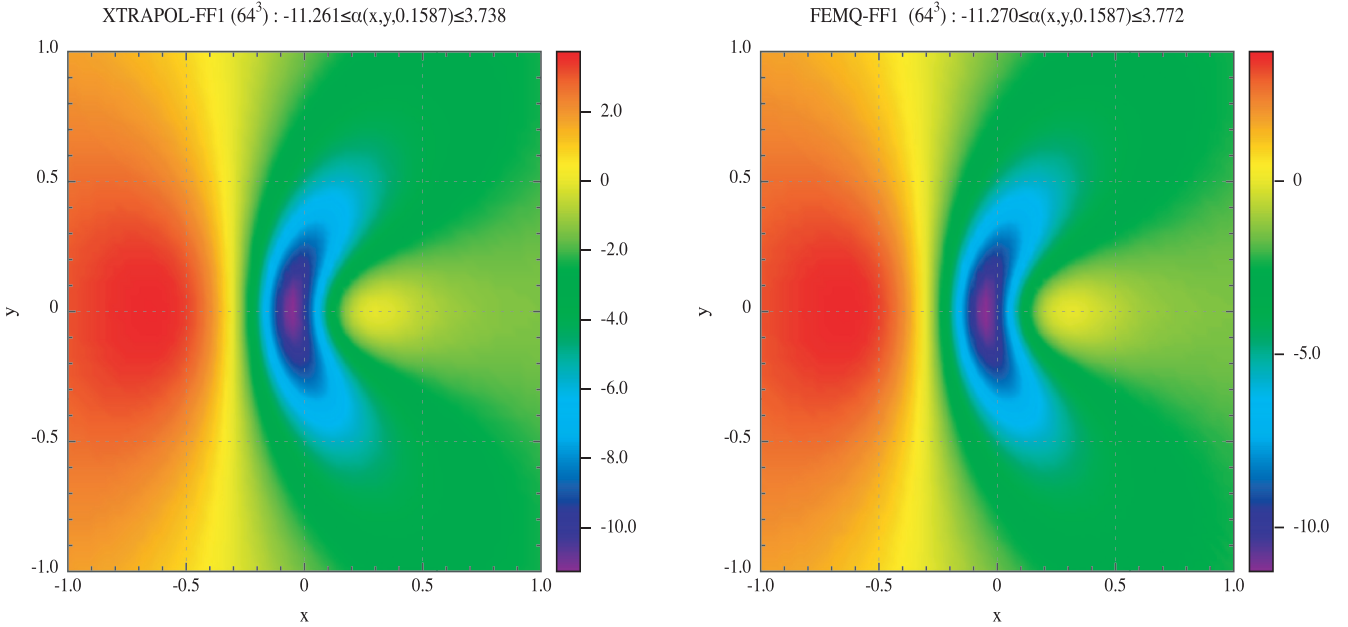

Fig. 6. Distribution of α on the plane $\{z = 0\}$ for the particular force-free solution FF1 (*left panel* of Fig. 1), and the approximated solutions obtained with XTRAPOL (*left panel*) and with FEMQ (*right panel*) at the same numerical resolution of 64^3.

5. Test cases

In this section, we introduce the exact solutions used later on to test and compare the two different approaches described above. To get them, we first consider the force-free field first derived in Low & Lou (1991) which is axisymmetric about some axis and has a singularity corresponding to a point source. With the same notations as in Amari et al. (1999), it writes in spherical coordinates

$$B_r = \frac{1}{r^2 \sin\theta} \frac{\partial A}{\partial\theta}, \tag{46}$$

$$B_\theta = -\frac{1}{r \sin\theta} \frac{\partial A}{\partial r}, \tag{47}$$

$$B_\phi = \frac{1}{r \sin\theta} Q, \tag{48}$$

where

$$A = \frac{P(\cos\theta)}{r^n}, \tag{49}$$

and

$$Q = aA^{1+\frac{1}{n}}, \tag{50}$$

with n an odd integer and a a real constant. P is then a solution to the boundary value problem

$$(1 - \cos^2\theta)\frac{d^2P}{d(\cos\theta)^2} + n(n+1)P + a^2\frac{1+n}{n}P^{1+\frac{2}{n}} = 0, \tag{51}$$

$$P(-1) = P(1) = 0, \tag{52}$$

and it can be shown to be uniquely determined if its number m of nodes is imposed a priori – i.e., $P = P(n, m)$.

Next we rewrite the field in the coordinates

$$X = x\cos\Phi - (z + L)\sin\Phi, \tag{53}$$

$$Y = y, \tag{54}$$

$$Z = x\sin\Phi + (z + L)\cos\Phi, \tag{55}$$

FF1 (64^3) : $-7.392 \leq \alpha(x,y,0.1587) \leq 2.445$

XTRAPOL (64^3) : $-7.352 \leq \alpha(x,y,0.1587) \leq 2.439$

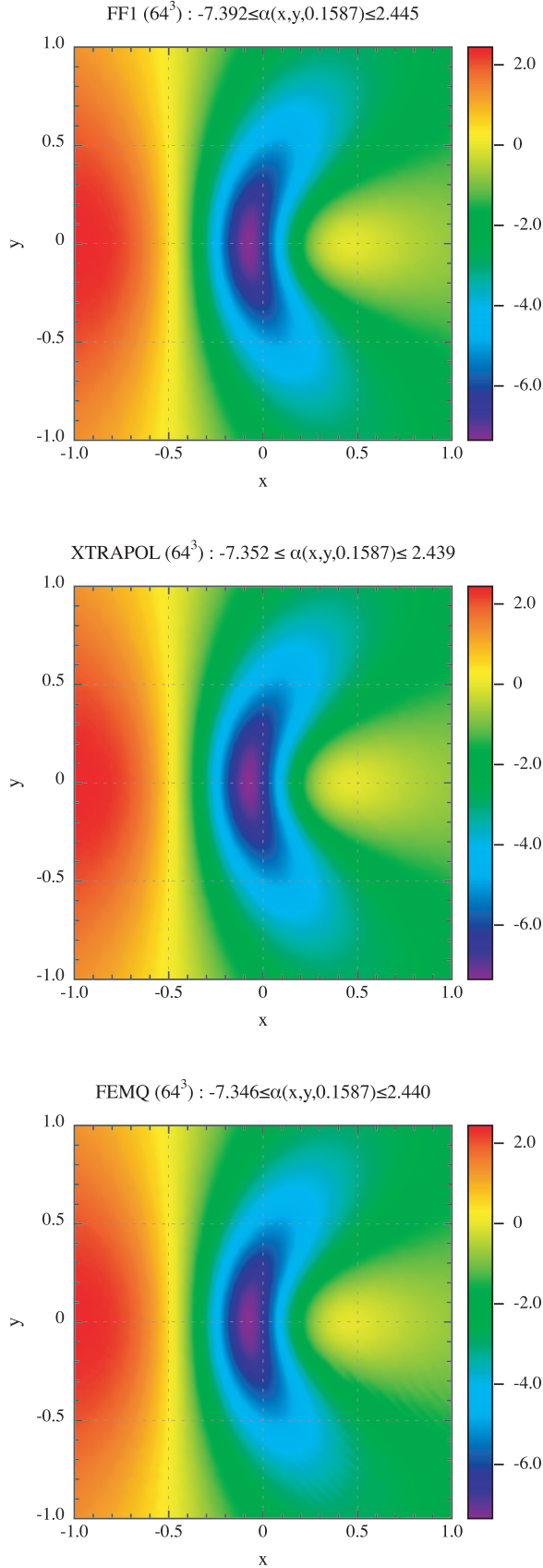FEMQ (64^3) : $-7.346 \leq \alpha(x,y,0.1587) \leq 2.440$

Fig. 7. Distribution of α on the plane $\{z = 0.1587\}$ for the particular force-free solution FF1 (*top panel*), and the approximated solutions obtained with XTRAPOL (*middle panel*) and with FEMQ (*bottom panel*) at the same numerical resolution of 64^3.

Table 1. Various error diagnostics (see text for definition) for comparison of XTRAPOL and FEMQ in the case of boundary data corresponding to FF1 and for a numerical resolution of 64^3. The values of the diagnostics for the reference case FF1 are displayed. The value of a norm of div B is also given since this is a key difference in the two approaches.

Model	VC	CS	NVE	MVE	$\| \text{div } \boldsymbol{B} \|_{L^\infty}$
XTRAPOL	0.9999	0.9999	0.0208	0.0162	0.53×10^{-14}
FEMQ	0.9999	0.9999	0.0097	0.0109	0.056

Table 2. Various error diagnostics (see text for definition) for comparison of XTRAPOL and FEMQ in the case of boundary data corresponding to FF2 and a numerical resolution of 64^3. The value of a norm of div B is also given since this is a key difference in the two approaches.

Model	VC	CS	NVE	MVE	$\| \text{div } \boldsymbol{B} \|_{L^\infty}$
XTRAPOL	0.9923	0.6981	0.2684	1.5444	0.44×10^{-14}
FEMQ	0.9927	0.6369	0.2631	1.0626	0.09

Table 3. Various error diagnostics (see text for definition) for XTRAPOL in the case of the reconstruction at the resolution of 128^3 of boundary data corresponding to FF1.

Model	VC	CS	NVE	MVE	$\| \text{div } \boldsymbol{B} \|_{L^\infty}$
XTRAPOL 128^3	0.99999	0.99999	0.0043	0.0058	0.15×10^{-13}

Table 4. Various error diagnostics (see text for definition) for comparison of XTRAPOL in the case of the reconstruction of boundary data corresponding to FF2 for the three numerical resolutions 64^3-128^3-192^3, showing the benefit of increasing the resolution.

Model	VC	CS	NVE	MVE	$\| \text{div } \boldsymbol{B} \|_{L^\infty}$
XTRAPOL (64^3)	0.9923	0.6981	0.2684	1.5444	0.44×10^{-14}
XTRAPOL (128^3)	0.9989	0.7630	0.1491	1.0331	0.14×10^{-13}
XTRAPOL (192^3)	0.9995	0.8326	0.0998	0.7443	0.17×10^{-13}

where $L > 0$ and Φ are given constants (the singular point is thus located at $(0, 0, -L)$). Restricting our attention to the part of space where $Z > 0$, we thus get in a half-space Ω a force-free field $\boldsymbol{B}$ without singularity which is fully determined by fixing the quadruplet (n, m, L, Φ). Unlike in Amari et al. (1999) where a unique test solution was built up, we consider here two solutions (referred to as FF1 and FF2 hereafter) corresponding to two different ranges of nonlinearity. They are defined by the choices $FF1 := (n = 1, m = 1, L = .3, \Phi = \pi/4)$ and $FF2 := (n = 3, m = 1, L = .3, \Phi = 4\pi/5)$, and their distributions of B_z and α on $\{z = 0\}$ are shown in Figs. 1 and 2, respectively.

These two solutions allow us to target two ranges of theoretical electric current distributions. Indeed, both the current intensity and the length scale of variation of α compared to that of B_z are larger for FF2 than for FF, as seen in Figs. 1 and 2. FF2 thus represents an extreme test for the reconstruction methods.
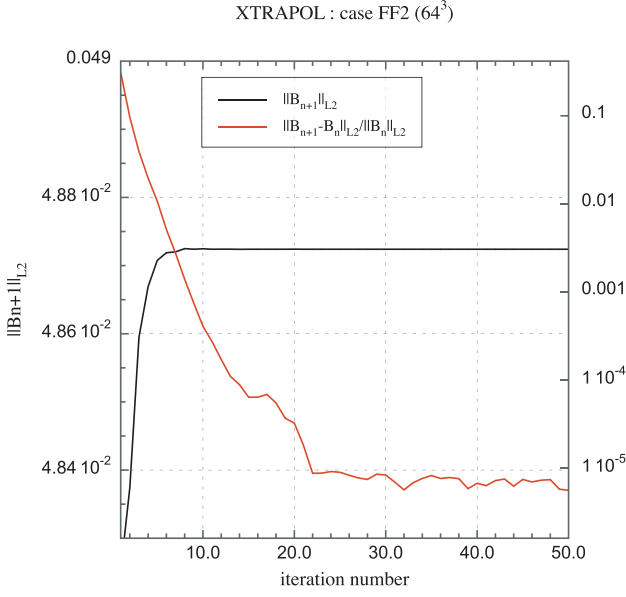
XTRAPOL : case FF2 (64^3)

Fig. 8. Convergence properties of the method XTRAPOL applied to the extreme nonlinear case FF2 with numerical resolution of 64^3. The rate of convergence of the sequences is close to exponential up to about 10^{-4} and decreases up to 10^{-5}, while the norm of the solution has reached its asymptotical value in about 15 iterations. Further decrease of the rate of convergence is difficult to achieve.
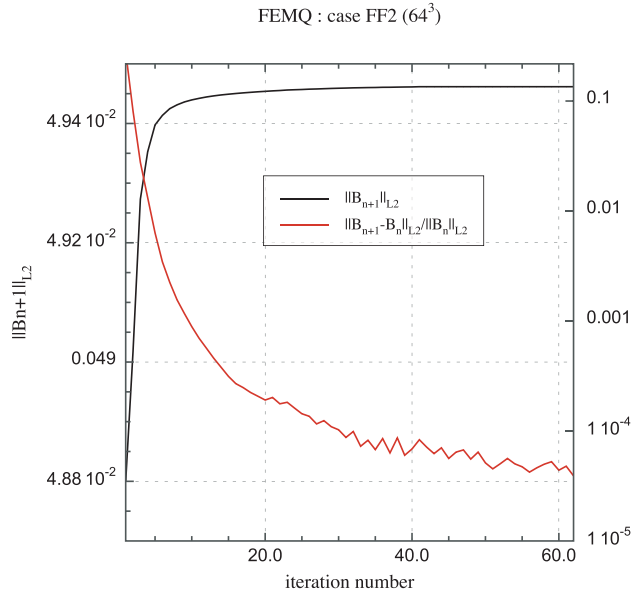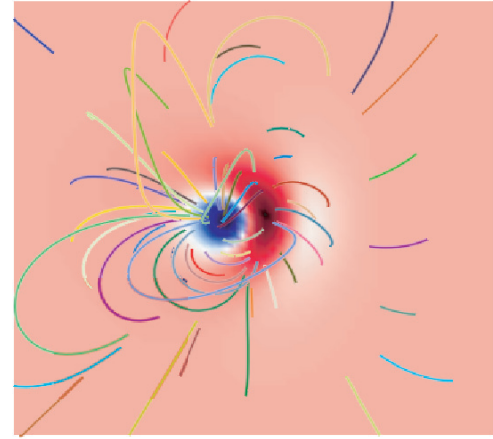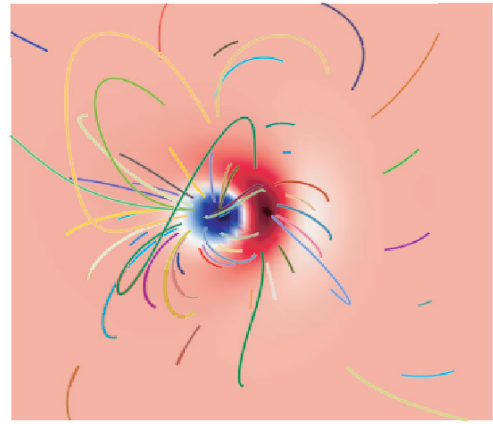

FEMQ : case FF2 (64^3)

Fig. 9. Convergence properties of the method FEMQ applied to case FF2 with numerical resolution of 64^3.

(a)

(b)

(c)

Fig. 10. Comparison of some field lines of the configurations corresponding to the case FF2 (panel **a**)) obtained with XTRAPOL (panel **b**)) and FEMQ (panel **c**)) for the same numerical resolution of 64^3.
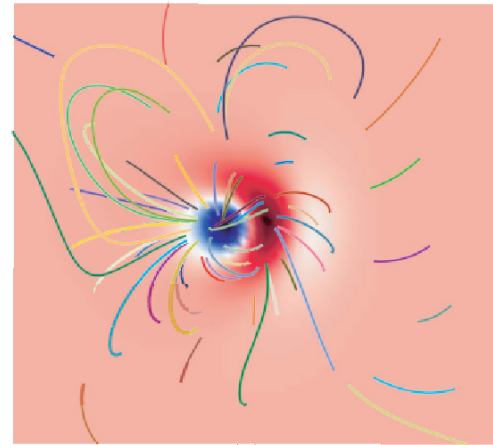
It is worth noting that although useful to compare the two reconstruction approaches, FF1 and FF2 exhibit a particular feature that is not often observed in photospheric vector magnetograms: the support of α is of the order of or larger than that of B_z while in general vector magnetograms reveal electric currents that are concentrated on a scale smaller than that of B_z. This represents a justification for testing on those solutions reconstruction approaches which allow for arbitrary non-zero distributions of B_n and particularly of α on all boundaries,

which was not the case in the method proposed in Amari et al. (1999), where we imposed $B_n = 0$ and $\alpha = 0$ on Γ_i, $\forall i \in (2, 6)$.

Finally it is important to notice that for both solutions above derived by the semi-analytical approach, there always remains a residual non-zero flux unbalance associated to a non-zero residual in div B. This residual depends on the numerical resolution used to derive the solutions and is found to be 1.5×10^{-2}

XTRAPOL-FF2 (64^3) : $-10.343 \leq \alpha(x,y,0.) \leq 11.113$ FEMQ-FF2 (64^3) : $-10.357 \leq \alpha(x,y,0.1587) \leq 11.072$
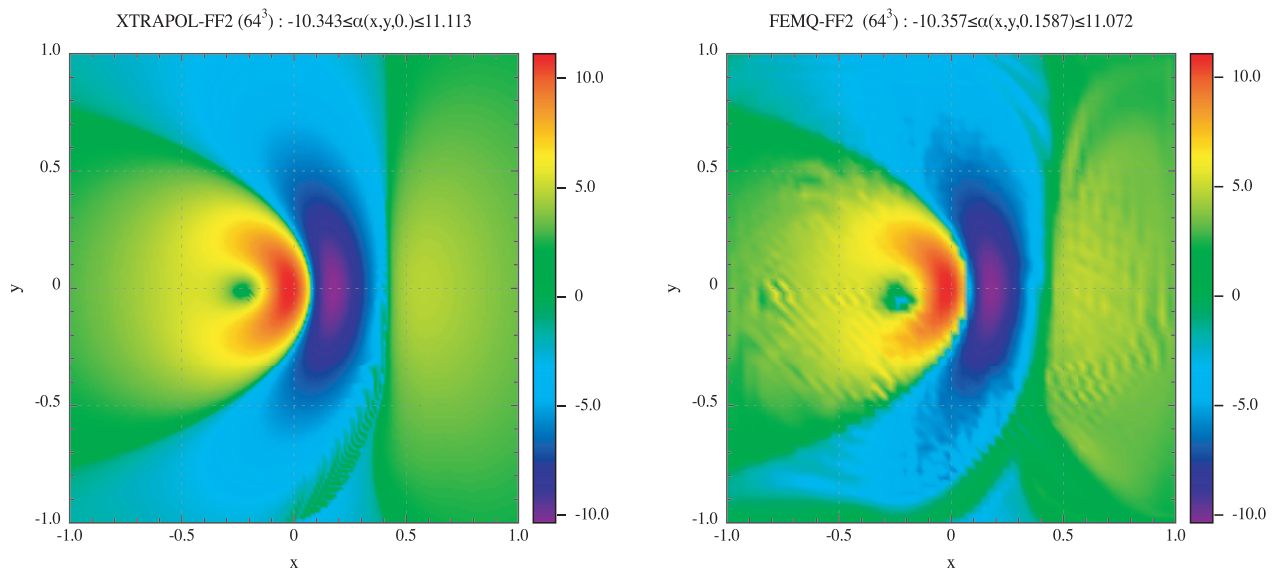

Fig. 11. Distribution of α on the plane $\{z = 0\}$ for the particular force-free solution FF2 (Fig. 2), and the approximated solutions obtained with XTRAPOL (*left panel*) and with FEMQ (*right panel*) at the resolution of 64^3.

for FF1 and 1.3×10^{-2} for FF2 for a resolution of (64^3). This unbalance problem always exists in data resulting from magnetograms for which flux-unbalances are often found to be even much larger. These small residual values do not represent a major issue, but should be added as a small source of errors, in particular for the first reconstruction approach XTRAPOL. As it will be seen in the next section, the latter keeps indeed div B to tiny machine round off errors, much below the residual values.

6. Results

6.1. Diagnostics

The error diagnostics used for the comparison of the two approaches are identical to those defined in Schrijver et al. (2005). Let u and v be two vectors, and N be the number of computational nodes. Then we introduce:

– The vector correlation

$$VC(u, v) = \frac{\sum_{i=1}^{N} u_i \cdot v_i}{\sqrt{\sum_{i=1}^{N} |u_i|^2} \sqrt{\sum_{i=1}^{N} |v_i|^2}}. \tag{56}$$

– The Cauchy-Schwartz correlation

$$CS(u, v) = \frac{1}{N} \sum_{i=1}^{N} \frac{|u_i \cdot v_i|}{|u_i||v_i|}. \tag{57}$$

– The Normalized Vector Error

$$NVE(u, v) = \frac{\sum_{i=1}^{N} |v_i - u_i|}{\sum_{i=1}^{N} |v_i|}. \tag{58}$$

– The Mean Vector Error

$$MVE(u, v) = \frac{1}{N} \sum_{i=1}^{N} \frac{|v_i - u_i|}{|u_i|}. \tag{59}$$

The various quantities above are evaluated for u equal to an exact solution – either FF1 or FF2 – and v equal to a numerical solution – obtained either with XTRAPOL or FEMQ. One clearly gets as reference values

$$VC(u, u) = CS(u, u) = 1, \tag{60}$$

$$NVE(u, u) = MVE(u, u) = 0. \tag{61}$$

As another measure of the quality of the solution we also found important to report estimates of div B, as well as estimates of α through few horizontal cuts. Those complementary indirect diagnostics are particularly important for formulations that do not correspond to well posed boundary value problem, because of overspecification of boundary conditions or constraints. Although the two formulations presented in this paper are well posed, we found useful to present such diagnostics.

We now describe the main results of our numerics. It is worth noticing that they have been obtained by running the codes on a single APPLE G5 desktop computer – a supercomputer is not needed.

6.2. XTRAPOL vs. FEMQ

To compare the two methods, we consider the two cases FF1 and FF2 reconstructed with the same numerical resolution of 64^3 nodes.

6.2.1. case FF1

Figure 3 shows the convergence properties of XTRAPOL with its rate of convergence in logarithmic scale, and the $L^2(\Omega_b)$ norm of the solution at each iteration, which is equivalent to the square root of the magnetic energy in non dimensional units. The rate of convergence is almost exponential even for this finite large scale distribution of α. Our convergence criterion $\epsilon = 10^{-6}$ is relatively strong since the magnetic energy
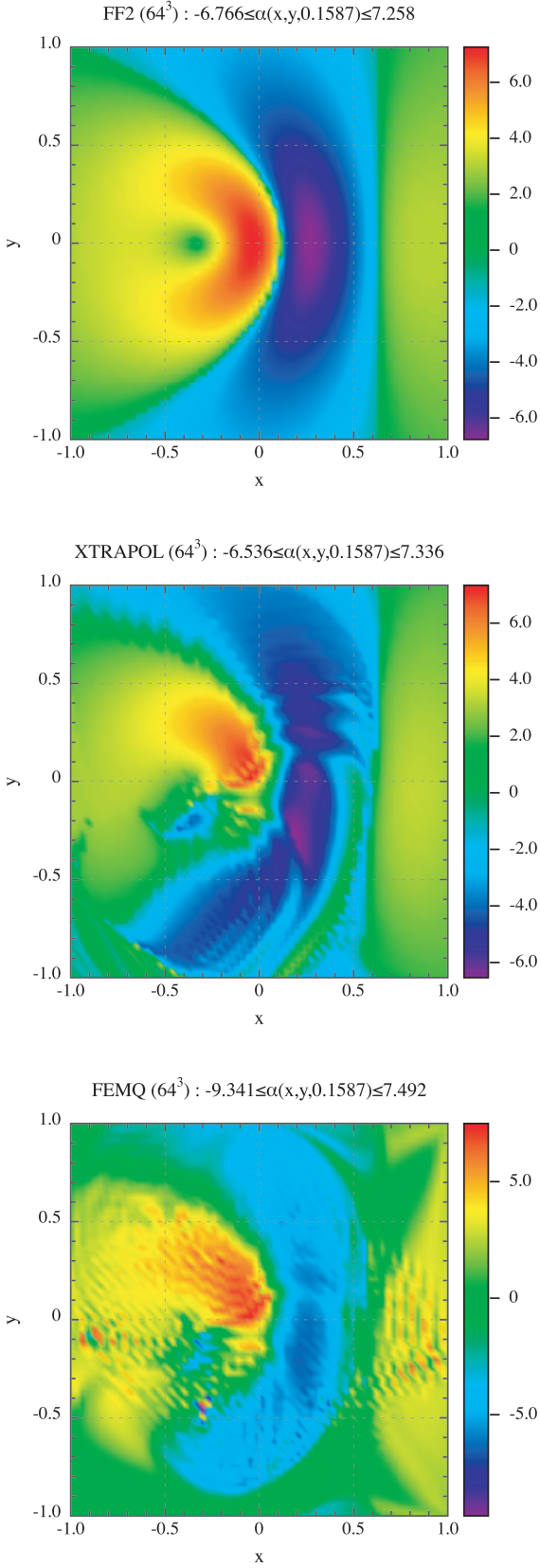
FF2 (64^3) : $-6.766 \leq \alpha(x,y,0.1587) \leq 7.258$

XTRAPOL (64^3) : $-6.536 \leq \alpha(x,y,0.1587) \leq 7.336$

FEMQ (64^3) : $-9.341 \leq \alpha(x,y,0.1587) \leq 7.492$

Fig. 12. Distribution of α on the plane $\{z = 0.1587\}$ for the particular force-free solution FF2 (*top left panel*), and the approximated solutions obtained with XTRAPOL (*top right panel*) and with FEMQ (*bottom left panel*) at the resolution of (64^3). The small ripples on the bottom panel confirm that the numerical errors are slightly larger for FEMQ than for XTRAPOL.
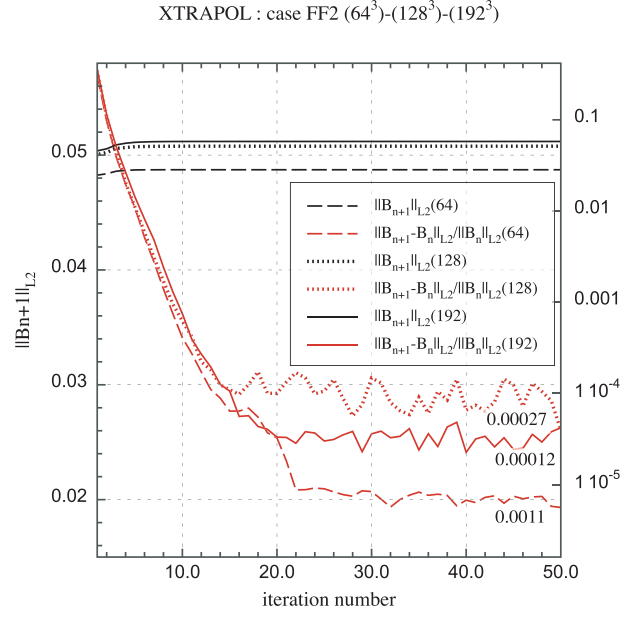
XTRAPOL : case FF2 (64^3)-(128^3)-(192^3)

Fig. 13. Convergence properties of the method XTRAPOL applied to the extreme nonlinear case FF2 with three different numerical resolutions (64^3, 128^3 and 192^3). The rate of convergence of the sequences is close to exponential up to about 10^{-4} and then oscillates at all resolution. Increasing numerical resolution does not improve the behaviour of this quantity. The norm of the solution (related to the magnetic energy) reaches rapidly its asymptotic limit which seems to be independent of the resolution. The number just below each curve indicates the relative L^∞ norm of the Lorentz force reached at the end of iterations, which show that increasing resolution leads to a better force-free final state.

(actually $\| B^{(n)} \|$) has already reached its asymptotic value at about iteration 15.

Figure 4 shows the evolution of the same quantities for the finite elements discretization FEMQ. Clearly, the same features do appear.

Figure 5 shows a qualitative comparison of some field lines (having the same footpoints positions) of the nonlinear solutions after convergence has been reached with XTRAPOL and FEMQ.

A more quantitative comparison performed using the error diagnostics defined in the previous subsection is shown in Table 1. It appears that the largest errors obtained for *NVE* and *MVE* are in the limit of a few percents, with slightly smaller errors for FEMQ whose solution reaches however a larger value for the divergence of $\boldsymbol{B}$.

Two cuts of α respectively at the bottom boundary (Fig. 6) and slightly above in the domain (Fig. 7), show that the errors are relatively small for α in $\partial\Omega_-$ (which is not imposed as a boundary condition). This confirms that XTRAPOL and FEMQ perform almost equally well.

6.2.2. case FF2

For this extreme case which is nonlinear on a large length scale, one can see in Fig. 8 the convergence properties of XTRAPOL. In this case the norm $\| B \|_{L^2}$ (and then the magnetic energy)
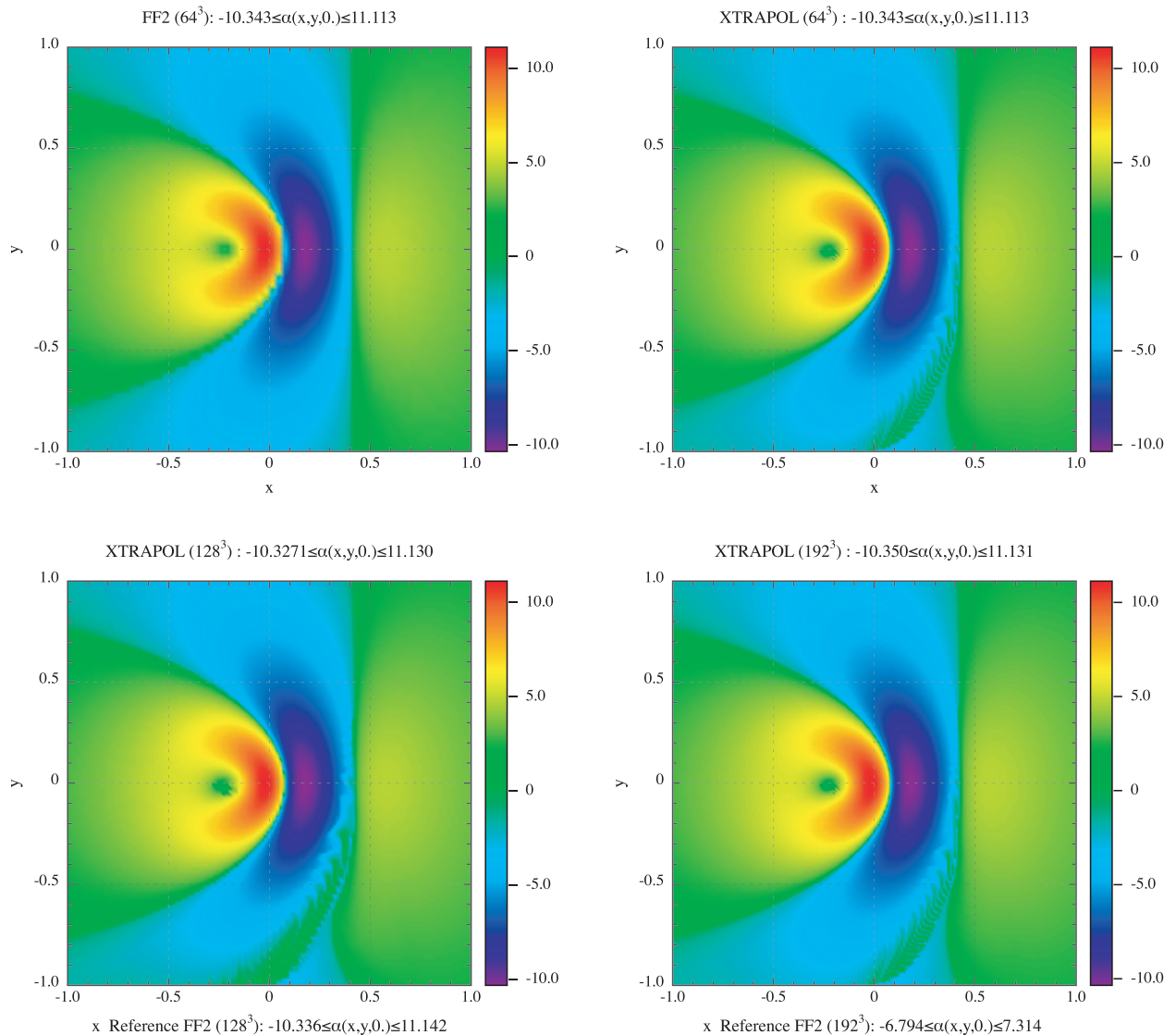
Fig. 14. Distribution of α on the plane $\{z = 0.\}$ for the particular force-free solution FF2 (see text) obtained with XTRAPOL at three numerical resolutions: 64^3-128^3-192^3.

has reached quickly its asymptotical value (iteration 10) inside the region of exponential decrease of the rate of convergence (up to iteration 15). The rate of convergence decreases up to about 10^{-5}. However, unlike for FF1, beyond 10^{-5} it is more difficult to decrease the rate of convergence in order to achieve our strong convergence criteria (at this resolution) of 10^{-6}. As seen in Fig. 9 this kind of behaviour is even worse for FEMQ since convergence up to 10^{-4} is even slower and not exponential (unlike for XTRAPOL), and after more than 60 iteration the rate of convergence seems to saturate around a value that does not reach 10^{-5}. It is worth noting that added to the oscillations observed in the rate of convergence for FEMQ we found that the number of iterations used to reach the solution of the linear system associated to the computation of α with FEMQ suffers some other oscillations. This behaviour is not observed with XTRAPOL for which α is computed by following the characteristics. Although for both methods the norm $\| B \|_{L^2}$ converges rapidly towards its asymptotical value, the corresponding two solutions reached after 50 iterations for

XTRAPOL and 60 iterations for FEMQ exhibit a difference of about 7×10^{-4} for this norm.

Let us however look at the configurations obtained after the rate of convergence is below 10^{-5} for XTRAPOL and 10^{-4} for FEMQ. Figure 10 shows some field lines of the configurations obtained with XTRAPOL and FEMQ. It appears that the matching with the exact solution FF2 is not as good as it was in the case FF1 at this resolution of 64^3. More quantitative measures of the errors are given in Table 2. They do clearly show that FEMQ and XTRAPOL perform almost equally for the reconstruction of this extreme case apart for the divergence of B, although the field lines of the two configurations obtained with both methods seem generally to agree, they show some differences. Those relative differences may be related to those previously observed in the norm $\| B \|_{L^2}$ of each solution as well as those in the divergence of B clearly related to the way each approach addresses the div $B = 0$ issue. It is moreover worth noticing that due to the oscillations in the computation step of α (for solving the non symmetric linear system), and
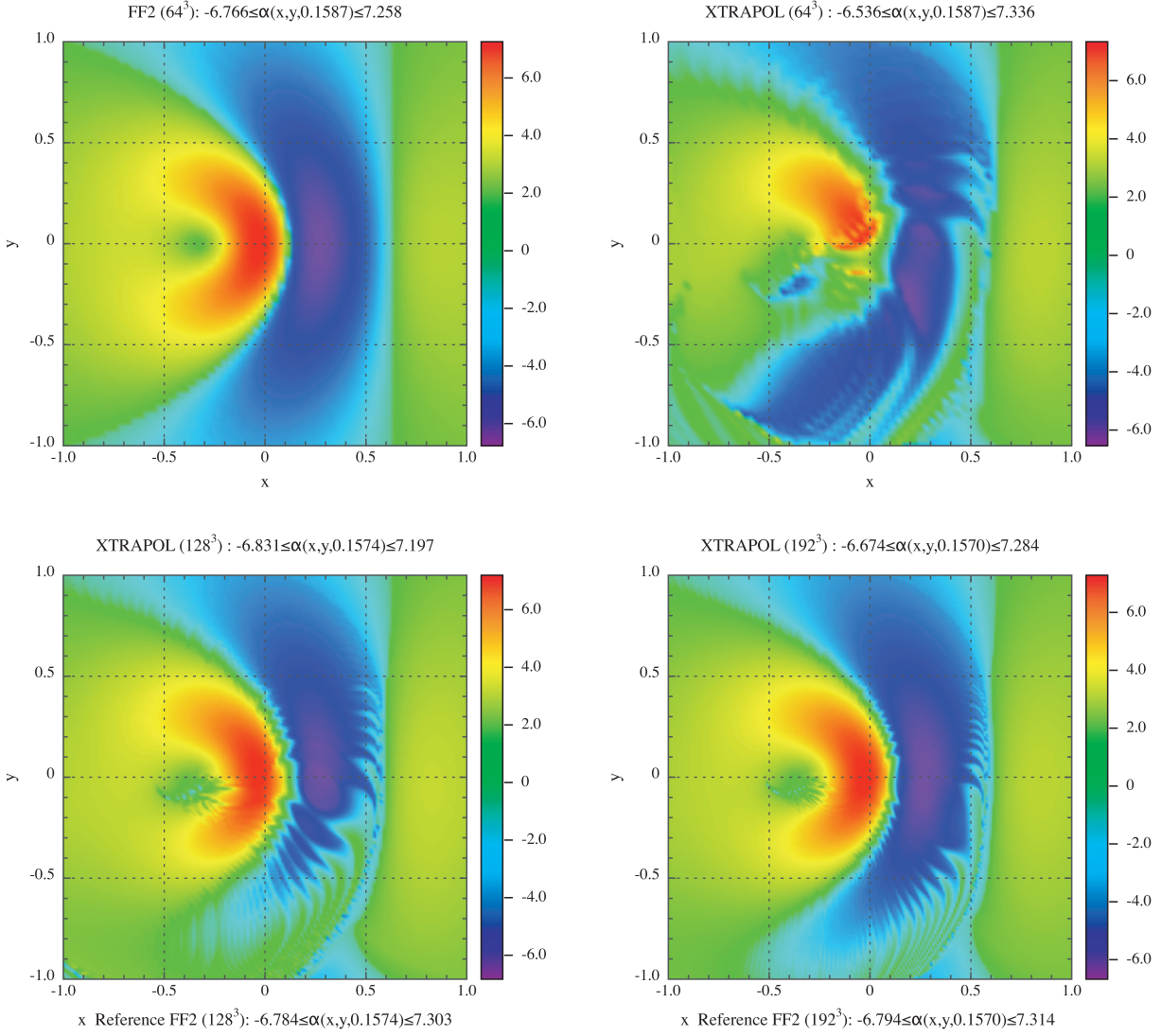
Fig. 15. Distribution of α around the plane $\{z = 0.1587\}$ for the particular force-free solution FF2 (see text) obtained with XTRAPOL at three numerical resolutions: 64^3-128^3-192^3.

the larger and non exponentially decreasing rate of convergence for FEMQ (even in the down to the 10^{-4} phase), this method appears to be slower than XTRAPOL for this extreme case FF2. This should however not be taken as a strong drawback since although the computations presented in this Paper were performed on a single processor machine, the fact that FEMQ used a linear system solver for computing α implies that this method requires much less effort to run on a parallel computer.

As for the case FF1 it is instructive to visualise the errors on α obtained at two heights after reconstructing equilibrium FF2 by the two methods (Figs. 11 and 12). One clearly sees that the mismatch, although not too large at the bottom boundary, is not small around $z = 0.15$.

6.3. Dependance on the numerical resolution: XTRAPOL

We now consider the effect of increasing the numerical resolution of the reconstruction calculation. Since we have shown

in the previous section that XTRAPOL performs faster than FEMQ and with a smaller rate of convergence for the case FF2, as well as for sake of computational time, we consider the effect of increasing the numerical resolution on the method XTRAPOL only. It is clear from Table 3 that increasing the numerical resolution to $128 \times 128 \times 128$ for the nonlinear case FF1 improves the already relatively good results obtained with XTRAPOL at the resolution 64^3.

When the numerical resolution is increased (64^3-128^3-192^3), the convergence diagnostics shown in Fig. 13 show that the rate of convergence still decreases fastly up to below 10^{-4}, but then oscillates for the case FF2, while $\| \boldsymbol{B} \|_{L^2}$ (square root of the magnetic energy) always converges rapidly towards a constant value independent of the numerical resolution.

However Table 4 shows a clear improvement of the error diagnostics for the solution obtained after XTRAPOL has reached its minimim rate of convergence. Similar improvements appear in the comparisons of the cuts of α at two heights for the reconstructed solution and the exact solution FF2 (Figs. 14 and 15), which shows better matching, and in the
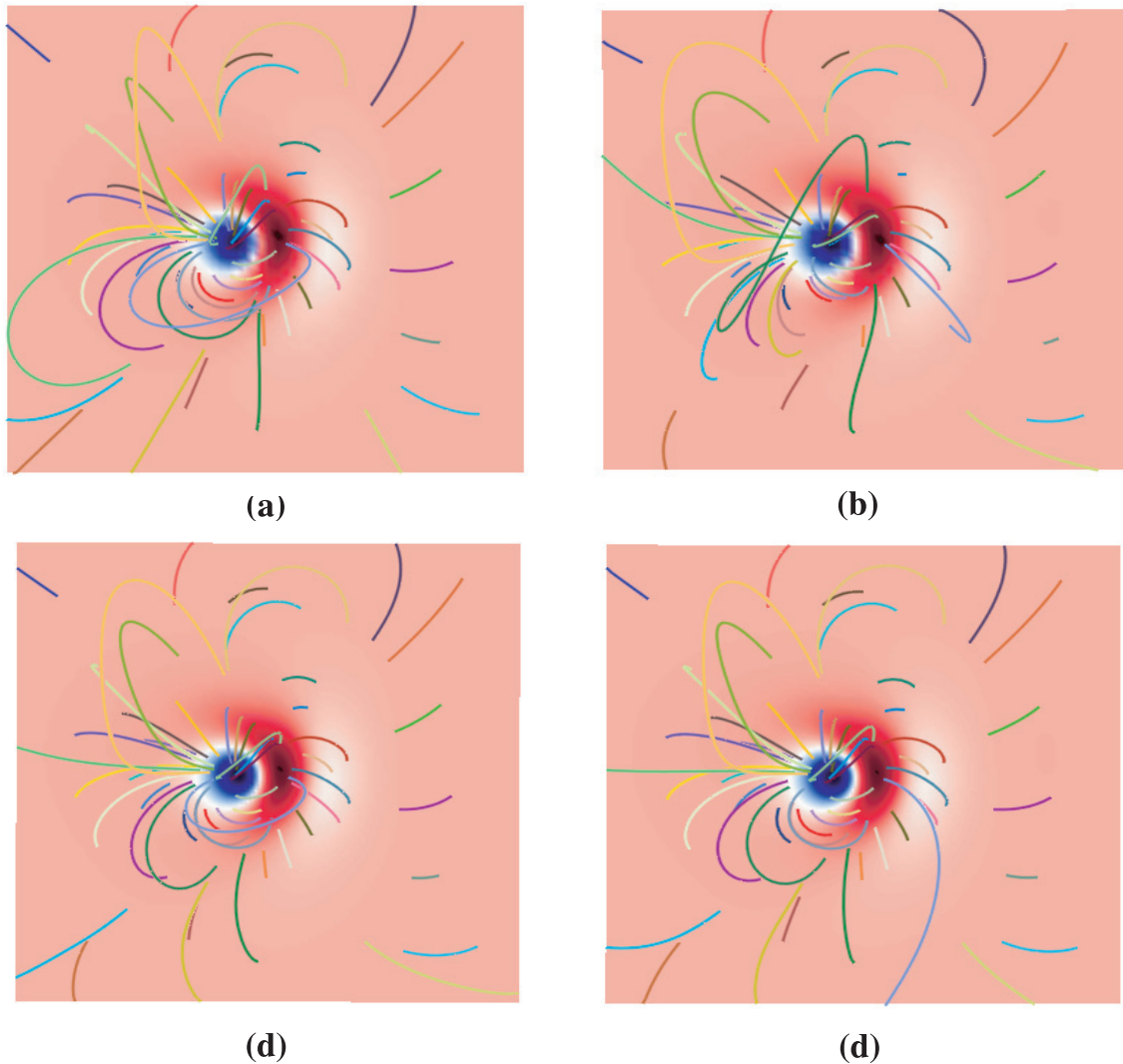
Fig. 16. Comparison of some field lines of the configurations corresponding to the case FF2 (panel **a**)) reconstructed with the model XTRAPOL at three numerical resolutions: 64^3 (panel **b**)), 128^3 (panel **c**)), and 192^3 (panel **d**)).

comparison of some field lines in Fig. 16. This confirms the conclusion from convergence diagnostics ($\|\boldsymbol{B}\|_{L^2}$) that increasing numerical resolution leads to a better approach of a somehow unique approximated solution, although the rate of convergence remains bounded.

7. Discussion and conclusion

In this paper we have considered two methods for reconstructing a force-free magnetic field in a bounded domain Ω_b from the given values of its normal component B_n on the boundary and of α on the part of this boundary where $B_n > 0$. Both methods have in common to rely on a well posed mathematical BVP and to belong to the class of iterative Grad-Rubin methods (Grad & Rubin 1958), in which two sequences of BVP are solved for $\boldsymbol{B}$ and α, respectively. However, they address two separate issues in different ways. The first one is the way the div $\boldsymbol{B} = 0$ constraint is solved. In the first method called XTRAPOL (first introduced in Amari et al. (1999)) a vector potential formulation allows to achieve this constraint

to round off machine errors, since $\boldsymbol{B}$ is defined in the kernel of the discretized operator div_h. On the contrary, the second method called FEMQ uses non-zero divergence finite elements, and a variational formulation of the ***curl*** − div system which minimizes the divergence of $\boldsymbol{B}$. The second difference lies in the way the BVP for α is solved. In the current version of XTRAPOL α is solved using a high order accurate characteristics scheme, while in FEMQ a global linear algebraic system associated with an hyperbolic BVP is solved. Further improvements of XTRAPOL with respect to its orignal version have been presented: introduction of a Poisson solver to achieve div $\boldsymbol{A} = 0$ to a high level of accuracy, and possibility to handle arbitrary non-zero distributions of B_n and α on the whole boundary of the domain (in Amari et al. (1999), it was assumed that $B_n = 0$ and $\alpha = 0$ on the faces of the domain, but the lower one).

To test and compare these methods, we have considered the particular semi-analytic exact solution derived in Low & Lou (1991). We have generated two solutions FF1 and FF2, corresponding to different distributions of b_0 and α_0 on the bound-

ary. For both solutions, α_0 is not small. FF2 actually represents an extreme nonlinear case in which α_0 is even larger, and on a scale much larger than the distribution of B_n (it is also larger for FF1). FF2 may be considered as a theoretical challenge to push the methods to their limits.

Our results show that for the case FF1, XTRAPOL and FEMQ perform relatively well for reconstructing the equilibrium at the numerical resolution of 64^3, with a slight advantage for XTRAPOL. The methods converge rapidly: the rate of convergence is close to exponential up to our strong limit criterion of 10^{-6}. However, for the extreme case FF2, FEMQ appears to have more difficulties to achieve fast convergence even up to 10^{-4}. For XTRAPOL, the convergence is exponential up to a rate of convergence of 10^{-4}, still decreases up to 10^{-5} and then oscillates, while the norm of the solution (related to the magnetic energy of the solution) clearly converges rapidly. The error diagnostics remain finite for both methods, with a larger value of the divergence of $\boldsymbol{B}$ for FEMQ which attempts to minimise this quantity while for XTRAPOL div $\boldsymbol{B} = 0$ is achieved to machine errors. Although FEMQ was found to be slower than XTRAPOL for the step of computation of α, in particular for the extreme case FF2, this should not be taken as a strong drawback. Indeed the fact that FEMQ uses a linear system solver for computing α implies that this method requires much less effort to run on a parallel computer. However we have not addressed this issue in scope of this Paper, in which we have presented only computations performed on a desktop single processor machine.

Increasing the resolution from 64^3 to 128^3 and 192^3 confirms that the norm of the approximated solution converges rapidly towards a unique constant value, and that the error diagnostics improve, but are still finite, while the rate of convergence keeps the same kind of behaviour.

Due to the existence of vector magnetic field ground measurements and the arrival of several solar space missions with onboard vector magnetographs, the reconstruction of the solar magnetic field from photospheric boundary data becomes an important valuable effort for the solar community. The results we have presented here may have some interest for this task. The first constraint on a reconstruction method is that it should be associated to a well posed boundary value problem. This is the case for the two methods we have presented here. Another constraint is that the methods should be able to tackle solar like flux and electric current distribution, implying in particular a knowledge of the limits of these methods for treating large electric currents. Since this issue could be addressed only on exact force-free solutions, we have considered one of the few known solutions (Low & Lou 1991). However, although this solution (FF2) represents a good challenge, it contains an awkward feature that is rarely present in true vector magnetograms: the length scale associated to the large value distribution of α is much larger than that of B_n while in the vector magnetograms that we have considered, we found a distribution of α more concentrated than that of B_n (Bleybel et al. 2002; Régnier et al. 2002; Régnier & Amari 2004). Therefore our conclusions on

the behaviour of our methods in this case (FF2) should be extrapolated to actual solar data with care. However, our numerical results could still give some feedback to solar data, since we have shown than increasing numerical resolution leads to improvement of the error diagnostics and fitting of the approximated solution. This result, although limited, may imply that in order to handle some of the active region current distributions, high enough resolution vector magnetographs should be necessary – which may be considered after all as a "Lapallissade" conclusion!

References

Aly, J. J. 1989, Sol. Phys., 120, 19

Amari, T., Aly, J., Luciani, J., Boulmezaoud, T. Z., & Mikic, Z. 1997, Sol. Phys., 174, 129

Amari, T., Boulmezaoud, T. Z., & Maday, Y. 1998, A&A, 339, 252

Amari, T., Boulmezaoud, T. Z., & Mikic, Z. 1999, A&A, 350, 1051

Bineau, M. 1972, Comm. Pure and Applied Math, 27, 77

Bleybel, A., Amari, T., van Driel-Gesztelyi, L., & Leka, K. D. 2002, A&A, in press

Boulmezaoud, T. Z., & Amari, T. 2000, Zeitschrift fur Angewandte Mathematik und Physik, 51, N 6, 942

Boulmezaoud, T. Z., & Amari, T. 2001, Mathematical and Computer Modelling, 34, 903

Brezis, H. 1983, Analyse fonctionnelle. Théorie et applications (Paris: Masson)

Buffa, A., & Ciarlet, P. J. 2001, Math. Meth. Appl. Sci., 24, 31

Chodura, R., & Schluter, A. 1981, J. Comp. Phys., 41, 68

Cuperman, S., Demoulin, P., & Semel, M. 1991, A&A, 245, 285

Demoulin, P., Cuperman, S., & Semel, M. 1992, A&A, 263, 361

Grad, H., & Rubin, H. 1958, in Proc. 2nd Intern. Conf. on Peaceful Uses of Atomic Energy, Vol. 31, United Nations, Geneva, 190

Kaiser, R., Neudert, M., & von Wahl, W. 2000, Commun. Math. Phys., 211, 111

Low, B. C. 2005, ApJ, 625, 617

Low, B. C., & Lou, Y. 1991, ApJ, 352, 343

Mikic, Z., & McClymont, A. 1994, in Solar Active Region Evolution - Comparing Models with Observations, Vol. ASP Conf Ser.

Régnier, S., & Amari, T. 2004, A&A, 425, 345

Régnier, S., Amari, T., & Kersalé, E. 2002, A&A, 392, 1119

Roumeliotis, G. 1996, ApJ, 473, 1095

Sakurai, T. 1981, Sol. Phys., 69, 343

Schrijver, C. J., DeRosa, M. L., Metcalf, T. R., et al. 2005, Sol. Phys., in press

Valori, G., Kliem, B., & Keppens, R. 2005, A&A, 433, 335

Wheatland, M. 2004, Sol. Phys., 222, 247

Wheatland, M., Sturrock, P., & Roumeliotis, G. 2000, ApJ, 540, 1150

Wiegelmann, T., & Neukirch, T. 2003, NonLinear Processes in Geophysics, 25, 19

Wu, S., Sun, M., Hagyard, M., & Gary, G. A. 1990, ApJ, 543620, 698

Yan, Y., & Sakurai , T. 2000, Sol. Phys., 195, 89